Remaining-useful-lifetime prediction of proton exchange membrane fuel cell considering model uncertainty quantification on the full-time scale

Xiaoran Yu, Yang Yang, Changjun Xie, *Member, IEEE*, Yang Li, *Member, IEEE*, Bo Zhao, *Member, IEEE*, Leiqi Zhang, Jie Song, Zhanfeng Deng, *Member, IEEE*

***Abstract*—A prognostics and health management (PHM) system with prediction at its core optimizes the durability of the proton exchange membrane fuel cell (PEMFC). However, the aging behavior model has some uncertainty due to limited knowledge, affecting the predictive performance in remaining useful life (RUL) prediction. To address this issue, an RUL prediction method based on the Bayesian framework considering uncertainty quantification on the full-time scale is proposed. Firstly, the state of health (SOH) of the PEMFC is estimated, and the behavior of uncertainty is quantified. Afterwards, a long short-term memory (LSTM) neural network is employed to make a prediction for its behavior. Finally, the RUL of PEMFC is predicted based on historical SOH and the predicted behavior of uncertainty. Validation indicates that the proposed method can make a long-term prediction and provide RUL prediction with high accuracy. Under the dynamic operating condition, in terms of long-term prediction, compared to unscented Kalman filter, adaptive unscented Kalman filter, double-input-echo-state-network and bidirectional LSTM, the proposed method decreases the error by 88.12%, 41.99%, 13.82% and 3.21%, respectively. And under the dynamic operating condition, the proposed method shows good stability. Moreover, the robustness of this method has also been verified.**

***Index Terms*—Bayesian framework, full-time scale, proton exchange membrane fuel cell (PEMFC), prediction of remaining useful life, uncertainty quantification.**

I. Introduction

In recent decades, traditional energy has faced the problems of depletion and environmental pollution, which have made the search for alternative energy become a hotspot [1]. Among kinds of technology of alternative energy, proton exchange membrane fuel cell (PEMFC) has gotten much research attention and is widely used due to its advantages of zero pollution, silent operation, and high energy conversion efficiency, becoming an excellent application in fields such as military, power, and transportation [2]. However, the short lifetime and expensive maintenance of PEMFC currently present significant challenges for its large-scale application [3]. Predicting the remaining useful life (RUL) of PEMFC can provide the necessary reference for operation, life extension, and maintenance strategies, which is crucial for promoting the commercial demonstration of PEMFC [4].

Currently, available methods include three types: model-based method, data-driven method and hybrid method [5].

Model-based method involves establishing a mathematical equation that comprehensively reflects the electrochemical mechanism of PEMFC based on the information of internal reaction. The equation is combined with specific algorithms to obtain accurate prediction. Model-based methods mainly involve the Kalman filter (KF), Particle filter (PF), mechanism model, and empirical model [6]. In [7], the extended Kalman filter (EKF) is applied to the heap test to estimate RUL, and the validation shows that EKF can give good RUL estimation for a parameter error of ±6%. However, the nonlinearity that EKF can handle is limited, and the Jacobian matrix is difficult to compute. Chen et al. utilized the unscented Kalman filter (UKF) and a voltage model to predict the aging of a PEMFC carried by a fuel cell electric vehicle (FCEV) under the actual operating condition. The experiment shows that this method has good robustness [8]. The computational efficiency can be greatly improved by processing data in batches. A good example is the frequency domain Kalman filter (FDKF) in [9]. FDKF processes the data by group in the frequency domain, improving computational efficiency while ensuring accuracy. PF can estimate errors, including systematic and random errors [10]. Its variants are also widely used [11], [12]. However, it faces problems of computational complexity and time consumption [8]. Obtaining comprehensive understanding of the aging mechanism of PEMFC is also a current research hotspot. Jouin et al. analyzed the factors affecting the power and lifetime of PEMFC [13]. They found that, the aging of electrodes and exchange membrane, is most closely related to the overall aging of the stack. They proposed a new mechanistic model and validated it on different datasets. Additionally, by building an empirical model with identified parameters, the relationships between aging parameters and operating conditions can be obtained [6]. The researchers

This work was supported by the National Key Research and Development Project of China (2020YFB1506802); and the Key Research and Development Project of Guangdong Province (2020B0909040004).

X. Yu are with the School of Automation, Wuhan University of Technology, Wuhan 430070, China.

Y. Yang, and C. Xie are with the School of Automation, Wuhan University of Technology, Wuhan 430070, China and also with Hubei Key Laboratory of Advanced Technology for Automotive Components, Wuhan University of Technology, Wuhan 430070, China (email: whutyangyang@whut.edu.cn; jackxie@whut.edu.cn).

Y. Li is with Department of Electrical Engineering, Chalmers University of Technology, Gothenburg 41258, Sweden.

B. Zhao and L. Zhang are with State Grid Zhejiang Electric Power Research Institute, Hangzhou 310014, China.

J. Song and Z. Deng are with Global Energy Interconnection Research Institute, Beijing 102211, China.

(*Corresponding authors: Yang Yang; Changjun Xie.*)

developed an empirical model of cathode aging for a PEMFC carried by an FCEV [14]. Kneer's team developed an electrochemically active surface area loss model which was used to predict the extent of Pt dissolution and estimate the aging state of the catalyst layer. Validation showed it could achieve high accuracy [15]. When PEMFC is considering as a whole device, internal parameters closely related to SOH, should change gradually, unlike external parameters which change drastically. It is easy to obtain the degradation law from these internal parameters, which is conducive to RUL prediction [16]. Therefore, it is necessary for RUL prediction to establish an aging behavior model.

Data-driven method involves directly learning the change of the target and automatically giving the required information based on currently sampled data and a large amount of historical data [17], mainly including echo state network (ESN) [18], adaptive neuro-fuzzy inference system (ANFIS) [19], nonlinear autoregressive exogenous neural (NARX) network [20], relevance vector machine (RVM) [21], gaussian process regressor (GPR) [22], and long-short-term memory (LSTM) neuro network [23]. It is useful to apply data-driven methods into RUL prediction of PEMFC [24]. Improved versions have been available. Due to the computational inefficiency of ESN with fixed output weights, a new ESN is developed, whose connective model between neurons are changed [25]. Its linear fitting process is faster. According to [26], the prediction horizon (PH) is an essential indicator of prediction, which is defined as the time from the start of the forecast to the end of the forecast. And long-term prediction requires PH greater than 168h. It provides sufficient time for strategy, so it has practical application value. To achieve long-term prediction, reference [27] utilizes an improved ESN to make long-term forecast for stack voltage. And the optimal combination of input parameters for operating conditions is studied. Wang et al. developed an LSTM driven by a navigation sequence, which generates a sequence to guide the LSTM's long-term forecast, making it more suitable for this task [28]. Data-driven methods require much data and have a long computational time. It is difficult to obtain relevant parameters for stable expression of SOH because only external parameters with poor robustness can be used.

Data-driven method relies on the quantity and quality of training data, while model-based method captures the changes of internal parameter but depends on the quality of the model. Therefore, hybrid method is proposed to combine the advantages of both methods. Multiple hybrid strategies exist. Some first decompose the voltage data into stable and unstable parts [29] or irreversible and reversible aging parts [30]. Different parts are handled by different algorithms, like the adaptive extended Kalman filter (AEKF) and NARX. To predict RUL, Liu et al. first used the particle optimization algorithm to optimize ANFIS to predict the trend of voltage, and then used the adaptive unscented Kalman filter (AUKF) to estimate RUL [31]. In [32], the model-based method which combines PF with an empirical model, and a NARX are used to make a prediction for the voltage separately, and then the results are weighted to be fused. [16] proposes EKF-LSTM to make a long-term forecast for both voltage and internal parameters. In most scenarios, the performance of the hybrid method is limited by the accuracy of the aging behavior model [26]. The model-based method is chosen in this paper.

Due to the limited availability of data on the aging mechanism of PEMFC, the established aging behavior models are partial [33]. Furthermore, the internal parameters of PEMFC are difficult to be directly measured during operation. They can be estimated indirectly, which introduces uncertainty. Uncertainty may arise from perturbation signals or dynamic model drift [34]. The measurement noise caused by perturbation signals needs to be considered [35]. The presence of undetected faults in PEMFC during operation can introduce uncertainty in the data, which is worth considering. For example, the water management state is affected by various operating conditions [36]. Inadequate water management measures can lead to failures. Membrane dry-out failure can reduce the conductivity of the membrane, and hinder the migration of protons to the catalyst layer. This results in a higher degree of activation polarization and irreversible membrane aging [37]. In addition, fuel shortage, low gas pressure, and excessive pressure in the back-pressure valve can also result in similar phenomena [2]. Issues, like the parameter identification algorithm getting trapped in the locally optimal solution, can lead to inaccuracy in model parameters. These facts indicate that the impact of uncertainty in PEFMC's RUL prediction is objective.

Since predictive outcomes may occasionally be unreliable, the absence of uncertainty quantification could render the method unable to provide confidence and assess the usability of the prediction [38]. Furthermore, reference [22] indicates that quantitative analysis of uncertainty aids in extracting aging-related information, and the uncertainty quantification in RUL prediction is currently an emerging research trend.

Currently, limited methods for quantifying uncertainty exist. Zhu et al. proposed a data-driven approach using a Bayesian Gated Recurrent Unit for short-term voltage prediction, taking into account the uncertainty of the neural network model. The algorithm demonstrates good robustness [39]. Reference [11] combines SVM with regularized particle filtering, adopting a similar framework as [16] to provide uncertainty characterization of RUL estimation in the form of probability distribution. The research mentioned above analyzes the uncertainty from the perspective of probability distributions. From the viewpoint of state-space equation, uncertainty can be considered as an external input to the system and can be estimated [40], [41]. Uncertainty sources include external disturbance, measurement noise, estimation algorithm characteristics, internal system dynamics and aging behavior models. These require further research.

To address uncertainty in RUL prediction and its challenges in mathematical modelling, specific matrices and parameters can be introduced into the process equation to account for state drift caused by uncertainty. This drift can be estimated in the historical stage, and it can be predicted in the prediction stage.

This article has been accepted for publication in IEEE Transactions on Transportation Electrification. This is the author's version which has not been fully edited and content may change prior to final publication. Citation information: DOI 10.1109/TTE.2023.3336324

A Bayesian RUL prediction method for PEMFC, incorporating uncertainty quantification on the full-time scale, is proposed. Historical SOH is estimated, and uncertainty is quantified based on the Bayesian framework from the perspective of state drift caused by uncertainty. The direction of state drift is determined and its degree is quantified. Based on the established direction and quantified degree in the historical stage, the degree of state drift caused by uncertainty is predicted by means of an LSTM optimized by dung beetle optimization algorithm (DBO-LSTM) in the prediction stage, so that the uncertainty is quantified on the full-time scale. RUL is predicted by combining quantified uncertainty, historical SOH, and the state-space model. Different from [39] and [11], uncertainty from aging behavior model is considered instead of the uncertainty from the algorithm. Different from [40] and [41], the form of uncertainty is considered unknown and is quantified from the state drift caused by uncertainty. The main contributions of this paper can be summarized as follows:

(1) In the historical stage, the Bayesian method is provided to assess the uncertainty behavior on the SOH estimation of PEMFC from the novel perspective, that is the state drift caused by uncertainty. The direction and degree of state drift are quantified,

(2) In the prediction stage, based on the historical uncertainty, uncertainty behavior is predicted by predicting the degree of state drift on the determined direction, and then is added to the process of SOH estimation, so that a model-based RUL prediction method considering uncertainty quantification on the full-time scale is constructed.

(3) Data from the static, quasi-dynamic, and dynamic operating conditions are used to verify the performance of the proposed method, and it is compared with UKF, AUKF, bidirectional LSTM (Bi-LSTM) and so on. Results show that it can make good RUL prediction under these operating conditions. Its robustness is also validated.

The organization of this paper is as follows: Section II presents the experimental setup. The specific details of the method are described in Section III. Section IV discusses the performance of the proposed method in long-term prediction and RUL prediction. Finally, Section V summarizes the article.

II. Experimental Setup

Experimental data for verifying the proposed method comes from 2 datasets: Dataset 1 and Dataset 2.

A. Dataset 1

Dataset 1 is from IEEE PHM 2014 [42]. Two ZSW BZ-100-13-5 PEMFCs are operated with auxiliary equipment, such as air supply device, sensor power unit and hydrogen supply device. Each stack is a 5-cell stack and its nominal operating current density is 0.7 A/cm^2. Each cell has an active aera of 100 cm^2. The maximum air flow rate is 100 L/min and the maximum hydrogen flow rate is 30 L/min. The first stack operates under the static condition with a constant current of 70A, called FC1. The other stack operates under the quasi-dynamic condition with a triangular ripple of ±10% added to the constant current of 70A at a frequency of 5kHz, called FC2. Feature tests, including polarization test and electrochemical impedance spectroscopy measurement, are conducted weekly. For FC1 and FC2, feature tests are conducted at different times. The fuel cell stacks need to be shut down during testing. A total of 24-dimensional data, including fuel cell voltage, current, and operating time, are recorded during the experiment. To optimize data complexity, fuel cell voltage and current density data are extracted every 1 hour of operation, as shown in Fig.1.

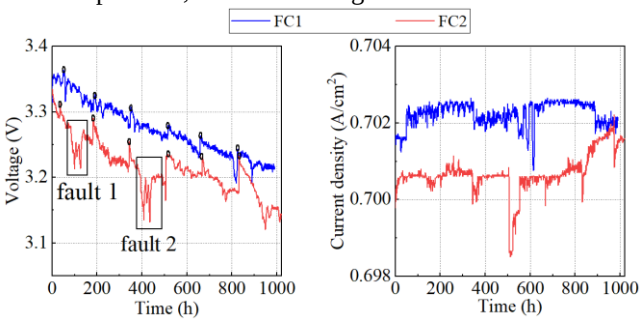

Fig.1 Experimental data of Dataset 1. (a) stack voltage of FC1 and FC2. (b) current density of FC1 and FC2.

From Fig.1, it is found that the voltage gradually decreases. Although the fuel cell voltage may recover to some extent after the feature tests, it ultimately converges into a declining trend [43]. The phenomena of voltage rising may be attributed to the recovery of water management and other reversible aging effects. FC2 experienced two failures during the operation process [16], which are shown in Fig.1(a).

B. Dataset 2

Dynamic operating condition is normal in real world, so a long-term dynamic aging experiment on a vehicle-oriental PEMFC single cell is designed with reference to the New European Driving Cycle [44]. The test station with internal controller is used to deploy the test. The experimental system includes the necessary equipment. The fuel cell is called FC3. It has an active aera of 25cm^2 and the operating temperature is 85℃. Its full load current is 35.6A. Both of the inlet-pressure of air and hydrogen gas are 110Kpa. The experiment can be considered as an In-situ accelerated stress test [4]. The experiment consists of 3076 cycles, accounting for approximately 1008 hours. Data is collected at a frequency of 1 Hz. The entire experimental voltage is shown in Fig.2(a) and the voltage and current in a single cycle are shown in Fig.2(b).

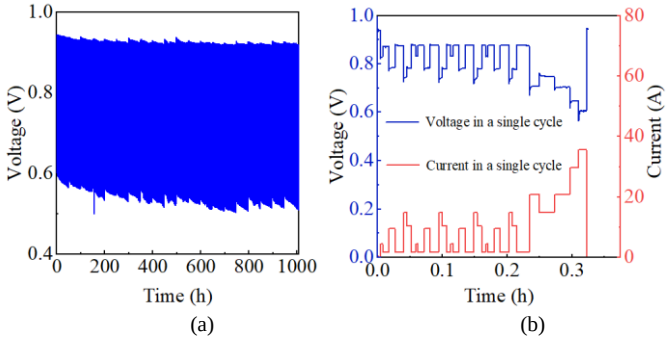

Fig.2 The experimental voltage of dynamic aging test. (a) The entire experimental voltage. (b) voltage and current in a single cycle

Its load current exhibits a clear hierarchical pattern, encompassing current level of 0A, 1.78A, 4.45A, 9.51A,

10.4A, 14.85A, 20.75A, 29.65A and 35.6A [45]. A pseudo-steady condition can be obtained by extracting the voltage at a current level [46]. Under this condition, the voltage shows an obvious decreasing trend which is easy to be captured by prediction algorithm [45]. Since the polarization curve model is applicable for estimating the SOH of PEMFC under the steady conditions, and PEMFC exhibits noticeable voltage degradation [45], the data of current level 1.78A is extracted from the experimental data, like reference [46]. Then, the sampling interval is fixed with 1h. Moreover, the data closest to the sampling time is extracted from the data of current level 1.78A to build Dataset 2, because the sampling frequency is so high that the actual sampling time is very close to the expected sampling time. It is a pseudo-steady condition selected from the dynamic condition, which encompasses aging information for PEMFC under the dynamic condition [46]. And its data complexity is optimized to make it suitable for the aging behavior model to be used. The experimental data of Dataset 2 is shown in Fig.3.

The voltage shows a clear downward trend for about 750 hours, The phenomena of voltage rising between 750h and 1008h can be attributed to improvement in the internal water management state of the fuel cell resulting from the implemented power reduction strategy which leads to changes in air pressure and flow rate [30], as well as a reduction in equivalent impedance [45].

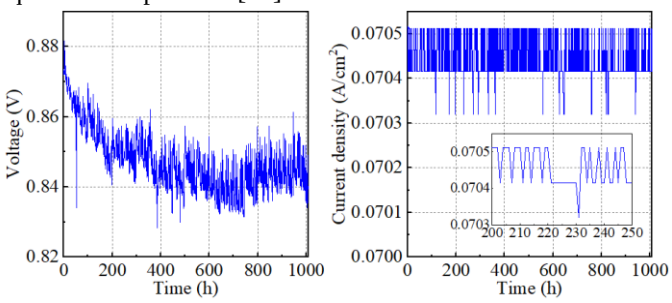

Fig.3 Experimental data of Dataset 2. (a) voltage. (b) current density

III. Methodology

The overall framework is shown in Fig.4. A position matrix ***d*** and parameter δ are introduced to construct a state-space model and Bayesian framework to express uncertainty behavior. Historical SOH is estimated, and the direction of state drift ***d*** is determined and the degree of state drift in the historical stage is estimated. The uncertainty behavior is quantified. DBO-LSTM is trained to predict δ in the prediction stage. The predicted δ, historical SOH, and process equation are combined to predict SOH and calculate RUL.

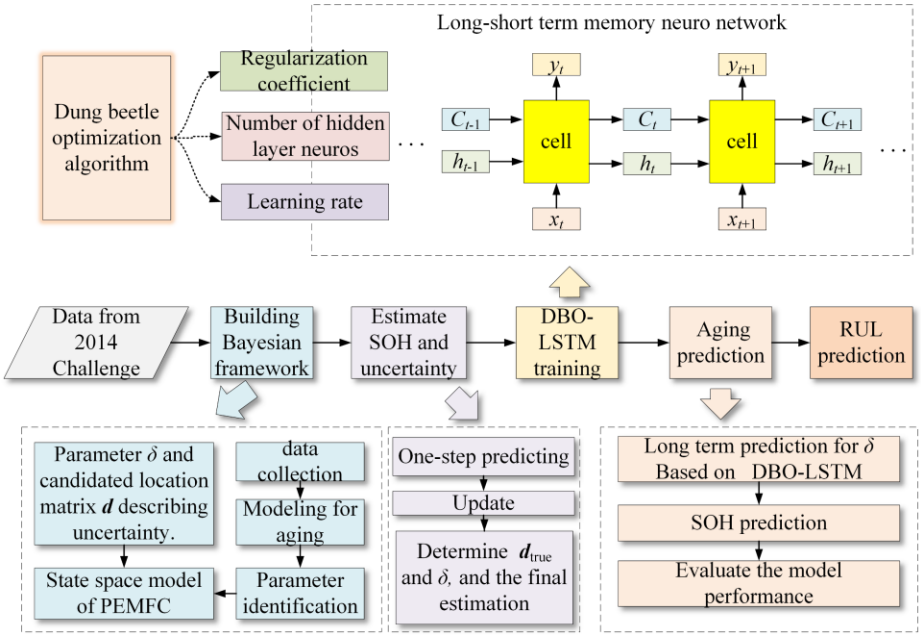

Fig.4 The framework of the proposed method.

A. Modeling for aging behavior

The foundation of RUL prediction is the aging behavior model, and the model here is as follows [7], [30], [31]:

$$V_{st} = n_{cell}(E_0 - R_{ohm} i - aT\ln(\frac{i}{i_0}) + bT\ln(1-\frac{i}{i_L}) \quad (1)$$

where V_{st} represents the stack voltage, n_{cell} denotes the number of the single cells, i denotes the current density, T denotes the stack temperature, a represents the Tafel constant, b represents the concentration constant. E_0 is the open circuit voltage of the stack at a given temperature and gas pressure, R_{ohm} is the total ohmic resistance, i_0 is the exchange current density, and i_L is the density of the limiting current.

According to [7], [30], [31], under the steady operating conditions, based on the parameter identification between (1) and polarization curve measured in the test, the parameters, R_{ohm} and i_L, exhibit significant changes, and their magnitude is comparable, while the changes in E_0 and i_0 are negligible. Dataset 1 belongs to the steady operating condition, and Dataset 2 belongs to the pseudo-steady condition [46]. Therefore, a single variable can be introduced to establish their relationship with time, which can serve as an indicator of

This article has been accepted for publication in IEEE Transactions on Transportation Electrification. This is the author's version which has not been fully edited and content may change prior to final publication. Citation information: DOI 10.1109/TTE.2023.3336324

SOH for the fuel cell, and the model can be established as follows [7], [30], [31]:

$$R_{\text{ohm}} = R_0(1+h(t)) \tag{2}$$

$$i_{\text{L}}(t) = i_{L0}(1-h(t)) \tag{3}$$

where $h(t)$ represents SOH, and its derivative $h'(t)$ represents the instantaneous aging rate. R_0 and $i_{\text{L}0}$ denote their initial values.

B. RUL prediction based on Bayesian framework

In this section, the fundamental principle of the RUL prediction method based on the Bayesian framework, which takes uncertainty quantification into account on the full-time scale, is described.

The state space model of PEMFC considered is as follows:

$$\begin{cases} \boldsymbol{x}_{m+1} = (A+\delta \boldsymbol{d}_i)\boldsymbol{x}_m + \boldsymbol{w}_m \\ y_m = g(\boldsymbol{x}_m, u_m) + v_m \end{cases} \tag{4}$$

In (4), $\boldsymbol{x}_m$ represents the state of the PEMFC system, where $\boldsymbol{x}_m = [h(m), h'(m)]^{\text{T}}$; y_m denotes the voltage measurement, $\boldsymbol{w}_m$ and v_m are the process noise and measurement noise, respectively, $g()$ represents observation equation, $g(\boldsymbol{x}_m, u_m) = n_{\text{cell}}(E_0 - R_0(1 + h(m))i_m - aT \times \ln(u_m / i_0) + bT \times \ln(1 - u_{\text{m}} / (i_{\text{L}0}(1 - h(m)))$, $u_m = i_m$; $\boldsymbol{w}_m$ and v_m are zero-mean random vectors following Gaussian distribution, with covariance $\boldsymbol{P}_0 > 0$, $\boldsymbol{Q}_m > 0$, $R_m > 0$. $\boldsymbol{A} = [1, T\text{s}; 0, 1]$, where $T\text{s}$ is the sampling frequency. The matrix $\boldsymbol{d}_i$ and the parameter δ jointly represent the behavior of uncertainty in the system. δ represents the degree of state drift, while $\boldsymbol{d}$ indicates the direction of state drift caused by model uncertainty, i.e., the position of δ within the state transition matrix. The elements of $\boldsymbol{d}$ are either 0 or 1. The Bayesian framework is as follows [34]:

$$\begin{aligned} &P(\delta, \boldsymbol{x}_m \mid \boldsymbol{d}_i, Y_{m-1}) \\ &= \int p(\boldsymbol{x}_m \mid \delta, \boldsymbol{x}_{m-1}, \boldsymbol{d}_i)(p(\delta, \boldsymbol{x}_{m-1} \mid \boldsymbol{d}_i, Y_{m-1}))d\boldsymbol{x}_{m-1} \end{aligned} \tag{5}$$

$$P(\delta, \boldsymbol{x}_m \mid \boldsymbol{d}_i, Y_m) \propto p(y_n \mid \boldsymbol{x}_m)\, p(\delta, \boldsymbol{x}_m \mid \boldsymbol{d}_i, Y_{m-1}) \tag{6}$$

$$p(\boldsymbol{d}_i \mid Y_m) = \frac{p(y_m \mid \boldsymbol{d}_i, Y_{m-1})\, p(\boldsymbol{d}_i \mid Y_{m-1})}{\sum_{i=1}^{L} p(y_m \mid \boldsymbol{d}_i, Y_{m-1})\, p(\boldsymbol{d}_i \mid Y_{m-1})} \tag{7}$$

$$p(\delta, \boldsymbol{x}_m \mid Y_m) = \sum_{i=1}^{L} p(\delta, \boldsymbol{x}_m \mid \boldsymbol{d}_i, Y_m)\, p(\boldsymbol{d}_i \mid Y_m) \tag{8}$$

where Y_m represents voltage measurement. y_m represents the voltage estimation. The prediction of the joint conditional probability density function of δ and $\boldsymbol{x}_m$ is made by (5), which is updated by (6). (7) estimates the probability of δ being at position matrix $\boldsymbol{d}_i$, and (8) combines the probability density functions and probability mass functions of δ at different predefined positions in the matrix $\boldsymbol{d}$.

Due to the lack of existing literature, δ is initialized to 1, and 15 possible positions are set as candidate positions where δ may occur, using permutation and combination, i.e. $\boldsymbol{d}_1$=[1, 0; 0, 0], $\boldsymbol{d}_2$=[0, 1; 0, 0], $\boldsymbol{d}_3$=[0, 0; 1, 0], $\boldsymbol{d}_4$=[0, 0; 0, 1], $\boldsymbol{d}_5$=[1, 1; 0, 0], $\boldsymbol{d}_6$=[1, 0; 1, 0], $\boldsymbol{d}_7$=[1, 0; 0, 1], $\boldsymbol{d}_8$=[0, 1; 1, 0], $\boldsymbol{d}_9$=[0, 1; 0, 1], $\boldsymbol{d}_{10}$=[0, 0; 1, 1], $\boldsymbol{d}_{11}$=[1, 1; 1, 0], $\boldsymbol{d}_{12}$=[1, 1; 0, 1], $\boldsymbol{d}_{13}$=[1, 0; 1, 1], $\boldsymbol{d}_{14}$=[0, 1; 1, 1], $\boldsymbol{d}_{15}$=[1, 1; 1, 1], $\boldsymbol{d} \in \mathbf{D} = \{\boldsymbol{d}_i, i = 1, 2, \ldots, L\}$, L = 15. To proceed with the subsequent procedures, Gaussian assumptions are made as follows [45]:

$$p(y_m \mid \boldsymbol{x}_m) \sim N(g(\boldsymbol{x}_m, u_m), R_m) \tag{9}$$

$$P(\delta, \boldsymbol{x}_m \mid \boldsymbol{d}_i, Y_m) \sim N\left(\begin{bmatrix} \delta_{i,m|m} \\ \boldsymbol{x}_{i,m|m} \end{bmatrix}, \begin{bmatrix} P^{\delta}_{i,m|m} & \boldsymbol{P}^{\delta x}_{i,m|m} \\ (\boldsymbol{P}^{\delta x}_{i,m|m})^T & \boldsymbol{P}^{x}_{i,m|m} \end{bmatrix}\right) \tag{10}$$

$$\begin{aligned} &p(\delta, \boldsymbol{x}_m \mid \boldsymbol{d}_i, Y_{m-1}) \\ &\sim N\left(\begin{bmatrix} \delta_{i,m|m-1} \\ \boldsymbol{x}_{i,m|m-1} \end{bmatrix}, \begin{bmatrix} P^{\delta}_{i,m|m-1} & \boldsymbol{P}^{\delta x}_{i,m|m-1} \\ (\boldsymbol{P}^{\delta x}_{i,m|m-1})^T & \boldsymbol{P}^{x}_{i,m|m-1} \end{bmatrix}\right) \end{aligned} \tag{11}$$

where, $\hat{\delta}_{i,m|m}$ and $\hat{\boldsymbol{x}}_{i,m|m}$ represent the updates at time step m, concerning the matrix $\boldsymbol{d}_i$.

One-step prediction, update, determination of historical $\boldsymbol{d}_{\text{true}}$ and final estimation, prediction for the behavior of uncertainty, and prediction for SOH are included in the proposed method.

Firstly, the following problem is defined based on (5) to study the one-step prediction of $\boldsymbol{x}$ and δ with the position matrix as $\boldsymbol{d}_i$.

$$\begin{bmatrix} \delta_{i,m|m-1} \\ \boldsymbol{x}_{i,m|m-1} \end{bmatrix} = \arg\max_{\delta, \boldsymbol{x}_m} p(\delta, \boldsymbol{x}_m \mid \boldsymbol{d}_i, Y_{m-1}) \tag{12}$$

Details are as follows [34]:

$$\delta_{i,m|m-1} = \delta_{i,m-1|m-1} \tag{13}$$

$$\boldsymbol{x}_{i,m|m-1} = (\boldsymbol{A} + \delta_{i,m-1|m-1}\boldsymbol{d}_i)\boldsymbol{x}_{i,m-1|m-1} \tag{14}$$

$$P^{\delta}_{i,m|m-1} = P^{\delta}_{i,m|m-1} \tag{15}$$

$$\boldsymbol{P}^{x}_{i,m|m-1} = \boldsymbol{G}_{m-1}\begin{bmatrix} P^{\delta}_{i,m-1|m-1} & \boldsymbol{P}^{\delta x}_{i,m-1|m-1} \\ (\boldsymbol{P}^{\delta x}_{i,m-1|m-1})^T & \boldsymbol{P}^{x}_{i,m-1|m-1} \end{bmatrix}\boldsymbol{G}^T_{m-1} + \boldsymbol{Q}_m \tag{16}$$

$$\boldsymbol{P}^{\delta x}_{i,m|m-1} = \begin{bmatrix} \boldsymbol{P}^{\delta}_{i,m-1|m-1} & \boldsymbol{P}^{\delta x}_{i,m-1|m-1} \end{bmatrix}\boldsymbol{F}^T_{m-1} \tag{17}$$

$$\boldsymbol{G}_{m-1} = \begin{bmatrix} \boldsymbol{d}_i \boldsymbol{x}_{i,m-1|m-1} & \boldsymbol{A} + \delta_{i,m-1|m-1}\boldsymbol{d}_i \end{bmatrix} \tag{18}$$

Then the prediction is updated. Voltage measurement Y_m is introduced, and $p(\delta, \boldsymbol{x}_m \mid \boldsymbol{d}_i, Y_{m-1})$ is updated to get $p(\delta, \boldsymbol{x}_m \mid \boldsymbol{d}_i, Y_m)$. Because the Gaussian assumptions (9) - (11) are satisfied, the problem of updating the one-step prediction can be converted into a nonlinear optimization problem as follows:

$$\begin{bmatrix} \delta_{i,m|m} \\ \boldsymbol{x}_{i,m|m} \end{bmatrix} = \arg\max_{\delta, \boldsymbol{x}_m} P(\delta, \boldsymbol{x}_m \mid \boldsymbol{d}_i, Y_m) \tag{19}$$

newton iteration method can be used to solve (19), and details are as follows:

The initiation of $\boldsymbol{\xi}$, $\boldsymbol{\xi}_{(0)\ i,m|m} = [\hat{\delta}_{\text{T}\ i,m|m-1}, \hat{\boldsymbol{x}}_{\text{T}\ i,m|m-1}]^{\text{T}}$, the maximum of iteration $iter_{\max}$=10, and the boundary condition is $|\boldsymbol{\xi}_{(iter)\ i,m|m} - \boldsymbol{\xi}_{(iter\_1)\ i,m|m}| < 0.01$. the formula is as follows:

$$\begin{aligned} &\boldsymbol{\xi}^{(iter+1)}_{i,m|m} \\ &= \boldsymbol{\xi}^{(iter)}_{i,m|m} - [\nabla^T_{\boldsymbol{\xi}}\boldsymbol{e}_i(\boldsymbol{\xi}^{(iter)}_{i,m|m}) \bullet \nabla_{\boldsymbol{\xi}}\boldsymbol{e}_i(\boldsymbol{\xi}^{(iter)}_{i,m|m}) + S_i(\boldsymbol{\xi}^{(iter)}_{i,m|m})]^{-1}\nabla^T_{\boldsymbol{\xi}}\boldsymbol{e}_i \\ &\bullet \boldsymbol{e}_i(\boldsymbol{\xi}^{(iter)}_{i,m|m}) \end{aligned} \tag{20}$$

where

$$\nabla_{\boldsymbol{\xi}}e_i = \begin{bmatrix} 0 & -R_m^{-\frac{1}{2}}\boldsymbol{C}^{(a)} \\ (\boldsymbol{P}^{\xi}_{i,m|m-1})^{-\frac{1}{2}} & \end{bmatrix} \tag{21}$$

This article has been accepted for publication in IEEE Transactions on Transportation Electrification. This is the author's version which has not been fully edited and content may change prior to final publication. Citation information: DOI 10.1109/TTE.2023.3336324

$$\boldsymbol{C}^{(a)} = \nabla_{\boldsymbol{x}} g\,|_{\boldsymbol{x}_{i,m|m}} = \left[n_{\text{cell}}(-R_0 i_m + bT(\frac{1}{1-h_{i,m}} - \frac{i_{L0}}{i_{L0}(1-h_{i,m}) - i_m})) \quad 0 \right] \tag{22}$$

$$\boldsymbol{P}^{\boldsymbol{\xi}}_{i.m|m} = [\boldsymbol{H} + (\boldsymbol{P}^{\boldsymbol{\xi}}_{i.m|m-1})^{-1}]^{-1} \tag{23}$$

$$\boldsymbol{P}^{\boldsymbol{\xi}}_{i,m|m-1} = \begin{bmatrix} P^{\delta}_{i,m-1|m-1} & \boldsymbol{P}^{\delta x}_{i,m-1|m-1} \\ (\boldsymbol{P}^{\delta x}_{i,m-1|m-1})^T & \boldsymbol{P}^{x}_{i,m-1|m-1} \end{bmatrix} \tag{24}$$

$$\boldsymbol{H} = \begin{bmatrix} 0 & 0 \\ 0 & (\boldsymbol{C}^{(iter)})^T R_n \boldsymbol{C}^{(iter)} \end{bmatrix} \tag{25}$$

$$\boldsymbol{S}_i(\boldsymbol{\xi}^{(iter)}_{i,m|m}) = \sum_{j=1}^{3} e_{i,j}(\boldsymbol{\xi}^{(iter)}_{i,m|m}) \nabla^2 e_{i,j}(\boldsymbol{\xi}^{(iter)}_{i,m|m}) \tag{26}$$

$e_{i,j}$ represents the element of the matrix.

After that the historical $\boldsymbol{d}_{\text{true}}$ is determined. The $\boldsymbol{d}_i$ that makes its $p(\boldsymbol{d}_i \mid Y_m)$ biggest is considered as $\boldsymbol{d}_{\text{true}}$ that can be expressed as follows:

$$\boldsymbol{d}_{true,m} = \arg\max_{\boldsymbol{d}_i \in \boldsymbol{D}} \mu_{i,m} \tag{27}$$

where $\mu_{i,m}= p(\boldsymbol{d}_i \mid Y_m)$, $\lambda_{i,m}=p(y_m \mid \boldsymbol{d}_i, Y_{m-1})$, and details are as follows [34]:

$$\mu_{i,m} = \frac{\lambda_{i,m}\mu_{i,m-1}}{\sum_{i=1}^{L} \lambda_{i,m}\mu_{i,m-1}} \tag{28}$$

where

$$\lambda_{i,m} = (2\pi)^{-\frac{1}{2}} |\Gamma_{i,m}|^{-\frac{1}{2}} \times \exp\left[-\frac{1}{2}(Y_m - g(\boldsymbol{x}_{i,m|m-1}))^T \Gamma_{i,m}^{-1} (Y_m - g(\boldsymbol{x}_{i,m|m-1})) \right] \tag{29}$$

$$\Gamma_{i,m} = \nabla_x g\,|_{\boldsymbol{x}_{i,m|m-1}} \boldsymbol{P}^{x}_{i,m|m-1} \nabla_x^T g\,|_{\boldsymbol{x}_{i,m|m-1}} + R_m \tag{30}$$

According to (8), the estimation of δ and $\boldsymbol{x}_m$ can be obtained by following formulas:

$$\boldsymbol{\xi}_{m|m} = \int \boldsymbol{\xi}_m p(\boldsymbol{\xi}_m \mid Y_m) d\boldsymbol{\xi}_m = \sum_{i=1}^{L} \mu_{i.m} \boldsymbol{\xi}_{i,m|m} \tag{31}$$

$$\boldsymbol{P}^{\boldsymbol{\xi}}_{m|m} = \int (\boldsymbol{\xi}_m - \boldsymbol{\xi}_{m|m})(\boldsymbol{\xi}_m - \boldsymbol{\xi}_{m|m})^T p(\boldsymbol{\xi}_m \mid Y_m) d\boldsymbol{\xi}_m = \sum_{i=1}^{L} \mu_{i.m} \left[\boldsymbol{P}^{\xi}_{i,mm} + (\boldsymbol{\xi}_{i,mm} - \boldsymbol{\xi}_{mm})(\boldsymbol{\xi}_{i,mm} - \boldsymbol{\xi}_{mm})^T \right] \tag{32}$$

Prediction for the behavior of uncertainty should be performed after historical SOH, $\boldsymbol{d}_{\text{true}}$ and δ are estimated in the historical stage. DBO-LSTM can be used.

LSTM is an improved version of the traditional RNN, capable of effectively capturing semantic relationships between long sequences and addressing the issue of long-term dependency. It retains important features of time series through various gate functions, mitigating gradient vanishing or exploding in long sequence tasks. Each unit of LSTM includes two memory states, controlled by input, forget, and output gates, one hidden state and one cell state. LSTM first removes a portion of information from the cell state using a forget gate. Then, based on the current state and the last unit's hidden state, necessary information is input into the next cell. The new hidden state is determined by the new cell state and input. DBO has been used for automatic optimization of LSTM to optimize the learning rate, regularization coefficient and number of neurons in the hidden layer.

The data of estimated δ in the historical stage are used to train DBO-LSTM. The trained network is then utilized to make a long-term prediction for the value of δ in the prediction stage based on the iterative configuration with sliding window [26]. It belongs to a long-term prediction for time-series data.

At the start of prediction t_{pre}, the data of $\{(t_{pre+1\text{-}v}, \delta_{pre+1\text{-}v}), (t_{pre+2\text{-}v}, \delta_{pre+2\text{-}v}), \ldots (t_{pre}, \delta_{pre})\}$ are input to the network to predict the value of δ at the next time $(t_{pre+1}, \hat{\delta}_{pre+1})$ at t_{pre+1}, the predicted δ, $\hat{\delta}_{pre+1}$ is introduced to the historical data to construct $\{(t_1, \delta_1), (t_2, \delta_2), \ldots (t_{pre}, \delta_{pre}), (t_{pre+1}, \hat{\delta}_{pre+1})\}$. Then, the data of $\{(t_{pre+2\text{-}v}, \delta_{pre+2\text{-}v}), \ldots (t_{pre}, \delta_{pre}), (t_{pre+1}, \hat{\delta}_{pre+1})\}$ are input to the network to predict the value of the next step $(t_{s+2}, \hat{\delta}_{pre+2})$. By that analogy, the prediction $\hat{\delta}_{pre+1}, \hat{\delta}_{pre+2}, \ldots \hat{\delta}_{pre+\text{PH}}$ all can be obtained. v is the width of the sliding window. The input of the DBO-LSTM is the δ sequence in the window before the prediction point, and the output is predicted δ at the time step. The iterative configuration is shown in Fig.5.

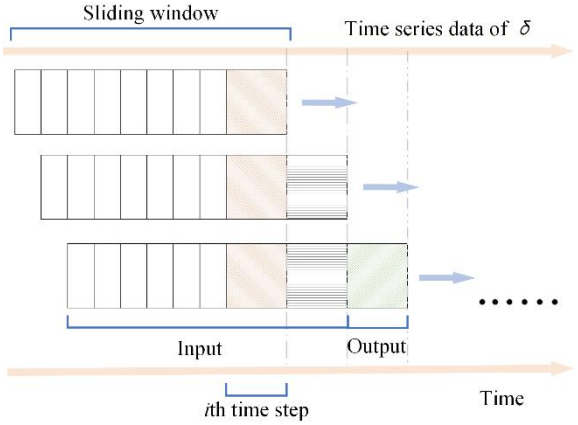

Fig.5 The iterative configuration with sliding window of DBO-LSTM

Finally, based on the prediction of parameter δ, historical SOH, and true position matrix $\boldsymbol{d}_{\text{true}}$, the future SOH is estimated using (33):

$$\boldsymbol{x}_{m+1} = (A + \delta_m \boldsymbol{d}_{\text{true}}) \boldsymbol{x}_m \tag{33}$$

The time between the start of prediction t_{pre} and time when the predicted SOH reaches the failure threshold is the predicted RUL. The time between the start of prediction t_{pre} and the end of life, t_{EOL} is the actual RUL

$$\text{RUL} = t_{EOL} - t_{\text{pre}} \tag{34}$$

Based on the previous discussion, the program execution flow of the proposed method is shown below.

TABLE I.
THE PROCESS OF THE PROPOSED METHOD

Algorithm 1 The process of the proposed method

Require: the maximum iteration number $a_{\max}$ and the total amount of historical data N
Ensure: RUL
1. Initialize the state $\boldsymbol{x}_n$ and its covariance $\boldsymbol{P}_x$, process noise $\boldsymbol{Q}$, measurement noise P, parameter δ and its covariance P_δ, and cross-covariance of $\boldsymbol{x}_n$ and δ, m =1, i =1
2. While ($m < N$) do
3. While $i < 15$ do
4. Make a prediction for $\boldsymbol{x}_{i,m}$ and $\delta_{i,m}$ based on (13)-(18)
5. Make an update for $\boldsymbol{x}_{i,m}$ and $\delta_{i,m}$ based on (20)
6. Compute the possibility $\mu_{i,m}$ based on (28)

7. Determine the true location matrix $\boldsymbol{d}_{\text{true}}$ based on (27)
8. End while
9. Obtain the estimation for $\boldsymbol{x}_m$ to get SOH and δ_m based on (31)-(32)
10. End while
11. Predict δ based on BDO-LSTM
12. RUL = 0
13. While (SOH < failure threshold) do
14. Compute the SOH at next time based on (33)
15. RUL+1
16. End while

IV. Discussion

The proposed method is compared with UKF, AUKF, double-input echo state network (DI-ESN), and bidirectional LSTM (Bi-LSTM). The long-term predictive performance of these five methods under different training set lengths is discussed using three metrics: Root Mean Square Error (RMSE), Mean Absolute Percentage Error (MAPE), and error of RUL (%Er_{RUL}). Accuracy (*Acc*) is used to evaluate the prediction accuracy of RUL over the entire lifecycle. Smaller values of RMSE, MAPE, and %Er_{RUL}, and larger values of *Acc* indicate higher accuracy of the prediction methods.

$$\text{RMSE} = \sqrt{\frac{\sum_{i=1}^{n}(y_i^{\text{pre}} - y_i^{\text{act}})^2}{n}} \tag{35}$$

$$\text{MAPE} = \frac{1}{n}\sum_{i=1}^{n}\left|\frac{y_i^{\text{pre}} - y_i^{\text{act}}}{y_i^{\text{act}}}\right| \tag{36}$$

$$\%\text{Er}_{\text{RUL}} = \frac{\text{RUL}_i^{\text{pre}} - \text{RUL}_i^{\text{act}}}{\text{RUL}_i^{\text{act}}} \tag{37}$$

$$Acc = 1 - \frac{1}{n}\sum_{i=1}^{n}\frac{\text{RUL}_i^{\text{pre}} - \text{RUL}_i^{\text{act}}}{\text{RUL}_i^{\text{act}}} \tag{38}$$

where, y_i^{act} represent the experimental data, y_i^{pre} represents the estimation or prediction, $\bar{y}$ represents the average of experimental data, $\text{RUL}_i^{\text{pre}}$ is the prediction of RUL at the time i, $\text{RUL}_i^{\text{act}}$ represents the true RUL at the time i. n represents the total amount of data.

A. Determination of failure threshold

The fuel cell's failure threshold should be determined. According to [7], [31], over the entire lifecycle, SOH exhibits an increasing trend with time. Moreover, its maximum $\text{SOH}_{\max}$ serves as the failure threshold, and its corresponding time is t_{EOL}.

SOH and the possibilities of different location matrices under static quasi-dynamic and dynamic operating conditions are estimated based on (13)-(32), as shown in Fig.6. Based on the setting forms of [7], [31], when the initial parameter setting is as follows, these methods can achieve good performance:

For FC1: R = 0.01, $\boldsymbol{Q}$ = [0,0; 0,10^{-10}], $\boldsymbol{x}_0$ = [0; 0.001], $\boldsymbol{P}_0$ = [0.01, 0; 0, 0.01].

For FC2: R = 0.01, $\boldsymbol{Q}$ = [0,0; 0,10^{-16}], $\boldsymbol{x}_0$ = [0; 0.001], $\boldsymbol{P}_0$ = [0.01, 0; 0, 0.01].

For FC3: R = 0.1, $\boldsymbol{Q}$ = [10^{-6},0; 0, 10^{-6}], $\boldsymbol{x}_0$ = [0; 0.001], $\boldsymbol{P}_0$ = [1, 0; 0, 1].

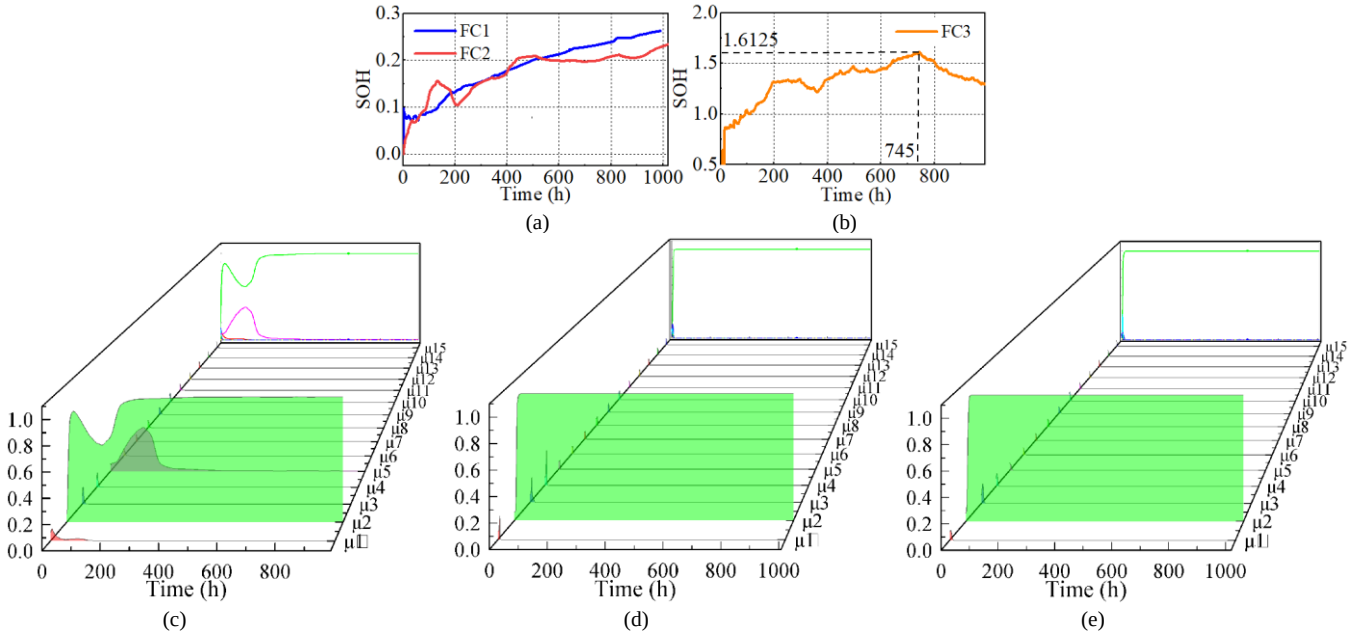

Fig.6 The estimated SOH and the possibilities of different position matrices in the aging test. (a) SOH, Dataset 1. (b) SOH, Dataset 2. (c) possibilities, FC1. (d) possibilities, FC2. (e) possibilities, FC3.

From Fig.6, it can be known that the true position $\boldsymbol{d}_{\text{true}}$ of parameter δ in the state transition matrix $\boldsymbol{A}$ is fast explicitly determined as $\boldsymbol{d}_2$. The possibilities of FC2 and FC3 are determined quicker than FC1, indicating that the behaviors of uncertainty on FC2 and FC3 are more apparent than FC1. For FC1, the failure threshold is 0.26239 and t_{EOL} is 991h. For FC2, the failure threshold is 0.23421 and t_{EOL} is 1020h. For FC3, the failure threshold is 1.6125 and t_{EOL} is 745h. It can be seen that lines of SOH under these operating conditions, all exhibit noticeable increasing trend, indicating the feasibility of the expression of SOH.

B. Performance of aging prediction of Dataset 1

To validate the proposed method's long-term prediction performance, the dataset is split into training and prediction sets. The training sets include 60% (FC1: PH = 397h, FC2: PH

This article has been accepted for publication in IEEE Transactions on Transportation Electrification. This is the author's version which has not been fully edited and content may change prior to final publication. Citation information: DOI 10.1109/TTE.2023.3336324

= 408h), 70% (FC1: PH = 297h, FC2: PH = 306h), and 80% (FC1: PH = 198h, FC2: PH = 204h) of the data, with the remaining part for prediction. The SOH trend is input into (1) for voltage prediction. The proposed method's performance is compared with UKF, AUKF, DI-ESN and Bi-LSTM. Long-term predictions of parameter δ are shown in Fig.7, and the voltage predictions are shown in Fig.8.

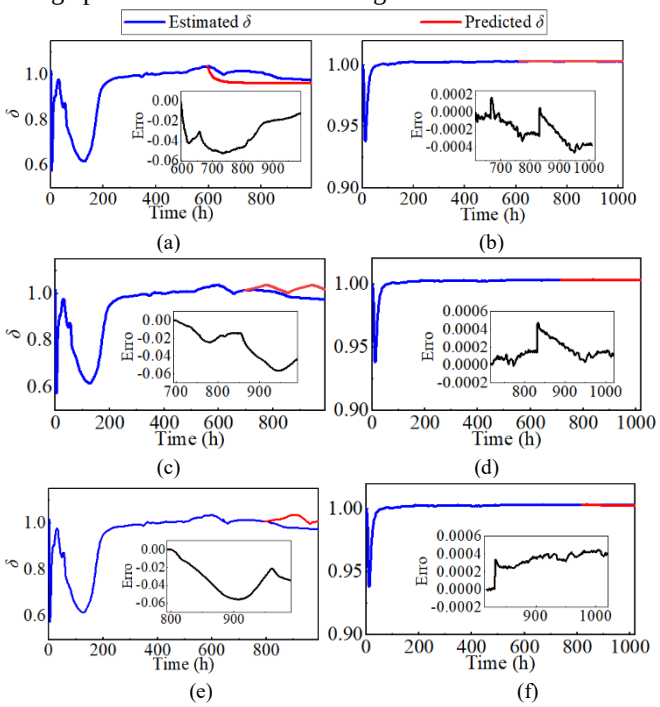

Fig.7 The comparison between estimated δ and predicted δ. (a) FC1, 60% training. (b) FC2, 60% training. (c) FC1, 70% training. (d) FC2, 70%. training (e) FC1, 80% training. (f) FC2 80% training.

It is shown that whether under the static condition or the quasi-dynamic condition, estimated δ can always reach a plateau, indicating that the proposed method has the ability to quantify the uncertainty behavior. For FC1, the maximum of estimated δ is about 0.97 while for FC2 the maximum of that is 1.00, which indicates that the aging behavior model under the quasi-dynamic condition has stronger uncertainty. For FC1, the error between the predicted and estimated values of δ is less than 0.06. For FC2, the error is less than 0.0004.

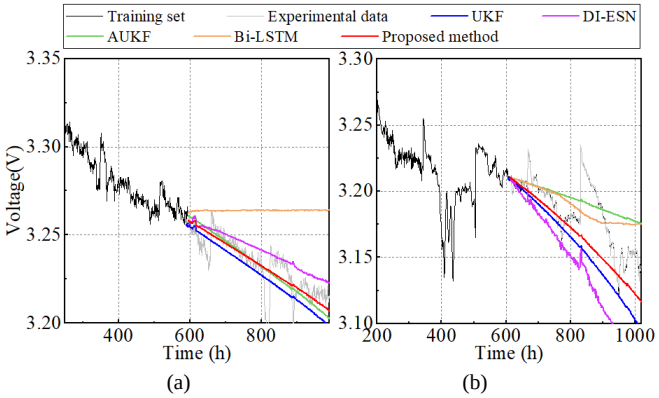

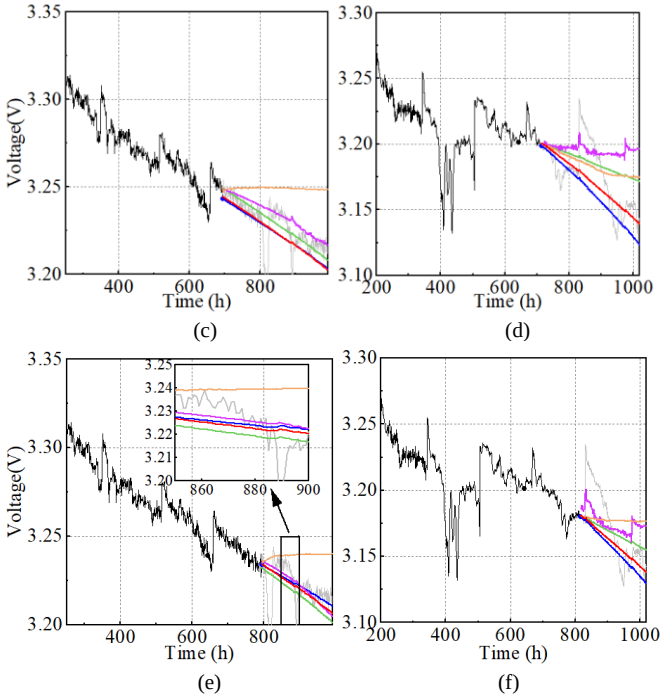

Fig.8 Long-term prediction results of different training set length. (a)FC1, 60% training. (b) FC2, 60% training. (c) FC1, 70% training. (d) FC2, 70% training. (e) FC1, 80% training. (f) FC2, 80% training.

It is shown that results of the proposed method, UKF, AUKF and DI-ESN exhibit obvious decreasing trends under the static condition but Bi-LSTM cannot. Under the quasi-dynamic condition, the proposed method can predict the degradation trend with different training sets. The results predicted by UKF, AUKF, DI-ESN and Bi-LSTM fail to guarantee the accuracy. And at 1020h, the prediction of the proposed method seems to be closest to the experimental data.

To compare the prediction accuracy of these methods, the RMSE, MAPE and $\%Er_{RUL}$ are listed in TABLE II.

TABLE II.
THE PRECISION OF DEGRADATION PREDICTION FOR FC1 AND FC2

		FC1			
		Proportion for training			Stacked value
Metric	Method	60%	70%	80%	
RMSE	UKF	0.0111	0.0101	0.0105	0.0317
	AUKF	0.0098	0.0092	0.0122	0.0312
	DI-ESN	0.0119	0.0109	0.0113	0.0341
	Bi-LSTM	0.0338	0.0245	0.0203	0.0786
	Proposed method	0.0090	0.0101	0.0110	**0.0301**
MAPE	UKF	0.0029	0.0025	0.0022	0.0076
	AUKF	0.0023	0.0018	0.0031	0.0072
	DI-ESN	0.0026	0.0021	0.0024	0.0071
	Bi-LSTM	0.0094	0.0065	0.0054	0.0213
	Proposed method	0.0020	0.0024	0.0025	**0.0069**
$\%Er_{RUL}$	UKF	-0.1864	-0.1611	-0.0754	-0.4229
	AUKF	-0.1741	-0.1319	-0.3584	-0.6644
	DI-ESN	-	-	-	-
	Bi-LSTM	-	-	-	-
	Proposed method	-0.0579	-0.1711	-0.1256	**-0.3546**
		FC2			
RMSE	UKF	0.0331	0.0228	0.0244	0.0803
	AUKF	0.0377	0.0431	0.0225	0.1033
	DI-ESN	0.0691	0.0301	0.0227	0.1219
	Bi-LSTM	0.0202	0.0219	0.0278	0.0699
	Proposed method	0.0246	0.0187	0.0224	**0.0657**
MAPE	UKF	0.0083	0.0053	0.0062	0.0198
	AUKF	0.0095	0.0108	0.0056	0.0259
	DI-ESN	0.0201	0.0078	0.0065	0.0344

	BI-LSTM	0.0050	0.0058	0.0077	0.0185
	Proposed method	0.0058	0.0042	0.0054	**0.0154**
	UKF	-0.4632	-0.3758	-0.5000	-1.339
	AUKF	0.4644	0.4459	-0.1478	1.0590
$\%Er_{RUL}$	DI-ESN	-	-	-	-
	BI-LSTM	-	-	-	-
	Proposed method	-0.2722	-0.0805	0	**-0.3527**

When the training proportion (TP) is 60%, the proposed method has the highest accuracy under the static condition. The proposed method reduces RMSE by 18.92%, 8.89%, 24.37% and 73.37% compared to UKF, AUKF, DI-ESN, and Bi-LSTM. The improvement is more significant on FC2. Compared with UKF, the proposed method reduces RMSE by 35.72%. The proposed method has one of the smallest stacked RMSE and MAPE for prediction results, regardless of operating conditions. Under the quasi-dynamic condition, compared with UKF, AUKF, DI-ESN and Bi-LSTM, the stacked RMSE of the proposed method is reduced by 17.93%, 36.21%, 46.10% and 6.00%, respectively. This is due to considering uncertainty quantification on the full-time scale, improving prediction performance for aging trends and RUL.

$\%Er_{RUL}$ is negative, indicating that the proposed method provides smaller RUL estimation than real RUL. This would provide enough time for maintenance. For FC2, the relative error in RUL prediction is smaller significantly than traditional methods. It enables long-term prediction up to PH = 408h, with relative error reductions of 41.23% and 41.38% compared to UKF and AUKF. At PH = 306h, the reductions are 78.58% and 81.95%. At PH = 204h, the predicted RUL by the proposed method is equal to the real RUL.

To comprehensively testify the performance of the proposed method under the static and quasi-dynamic conditions, results of other studies on the same dataset are listed in TABLE III. They are all data-driven methods. It can be seen that the proposed method can make prediction with lowest RMSE. Under the static condition, when the prediction starting point is 550h, the proposed method reduces RMSE by 28.82%, 27.98%, 55.35% and 63.44% compared with RVM [16], back propagation neural network (BPNN) [16], ESN [48] and NARX [30]. Under the quasi-dynamic condition, when the prediction starting point is 550h, the proposed method reduces RMSE by 39.56%, 17.80%, 48.81% and 54.88% compared with RVM, BPNN, ESN and NARX.

TABLE III.
COMPARISON WITH OTHER RESEARCHES IN RMSE FOR FC1 AND FC2

FC1			
	Prediction starting point		
Method	550h	650h	750h
RVM [16]	0.0170	0.0240	0.0127
BPNN [16]	0.0168	-	-
ESN [48]	0.0271	-	-
NARX [30]	0.0331	-	-
Proposed method	**0.0121**	**0.0185**	**0.0098**
FC2			
RVM [16]	0.0321	0.0572	0.0349
BPNN [16]	0.0236	-	-
ESN [48]	0.0379	-	-
NARX [30]	0.0430	-	-
Proposed method	**0.0194**	**0.0263**	**0.0212**

C. Performance of aging prediction of Dataset 2

Data is divided in the same way as the Dataset 1. The estimated δ and predicted δ are shown in Fig.9. The predictions made by UKF, AUKF, DI-ESN, Bi-LSTM and the proposed method are shown in Fig.10.

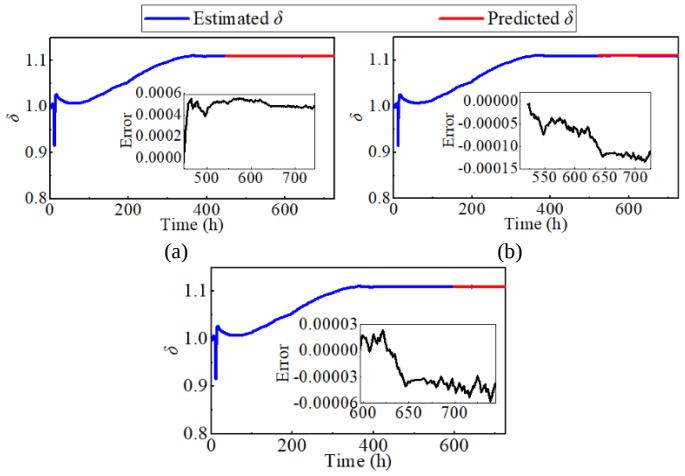

Fig.9 The estimated δ and predicted δ for FC3. (a) 60% training. (b) 70% training. (c) 80% training.

For FC3, the estimated value of δ eventually stabilizes at 1.1, indicating that under dynamic operating conditions, the uncertainty associated with the aging behavior model is greater than that under the static and quasi-dynamic conditions. When TP is 80%, the error between the predicted and estimated values of δ is less than 0.00003.

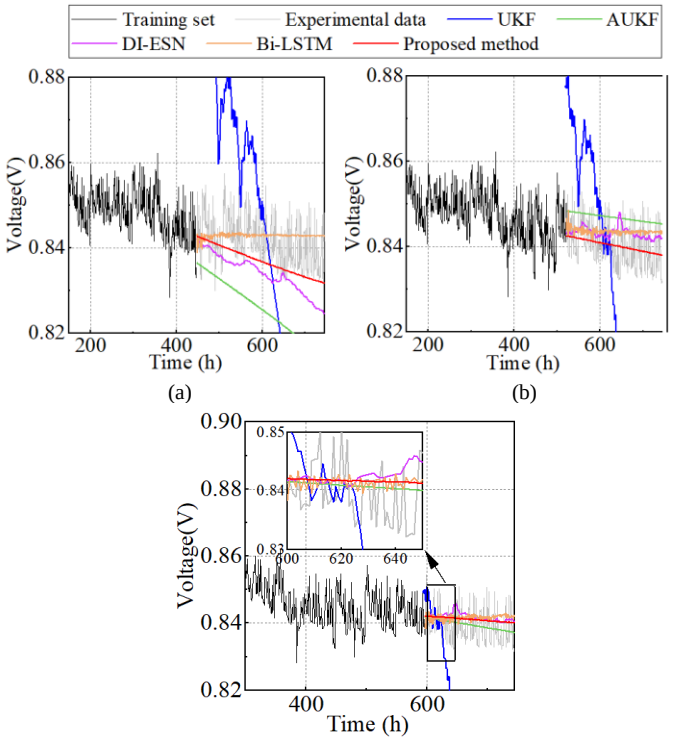

Fig.10 Long-term prediction results of FC3. (a) 60% training. (b) 70% training. (c) 80% training.

It is shown that UKF cannot give effective prediction. Parameter identification of polarization curve fitting is not applicable to dynamic conditions, and the aging behavior model is too simple for dynamic conditions, causing strong

This article has been accepted for publication in IEEE Transactions on Transportation Electrification. This is the author's version which has not been fully edited and content may change prior to final publication. Citation information: DOI 10.1109/TTE.2023.3336324

model uncertainty. For AUKF, the adaptive mechanism considers uncertainty from data and works a little so the predictive effectiveness is improved. But it can be found that when TP is 60% or 70%, the starting value of its voltage prediction is located at the edge of the experimental data, indicating that the state estimated by AUKF is not accurate.

For Bi-LSTM, with different TPs, the prediction has fluctuation and is difficult to exhibit a decreasing trend. This can be root in significant fluctuation in experimental data. It takes 750h for the experimental data to drop by 0.05V, during which the maximum fluctuation reaches 0.02V. In the whole experimental data, the voltage fluctuation is more significant than degradation. Therefore, the weights in Bi-LSTSM to store the volatility information are significantly higher than that to store the degradation information. When TP is 60%, prediction of DI-ESN exhibits decreasing trend but it deviates from the experimental data too much. When TP is 70% or 80%, DI-ESN is faced similar problem with Bi-LSTM.

TABLE IV.
THE PRECISION OF DEGRADATION PREDICTION FOR FC3

Metric	Method	Proportion for training 60%	70%	80%	Stacked value
RMSE	UKF	0.0487	0.0484	0.0553	0.1524
	AUKF	0.0175	0.0084	0.0053	0.0312
	DI-ESN	0.0092	0.0063	0.0062	0.0217
	BI-LSTM	0.0061	0.0065	0.0061	0.0187
	Proposed method	0.0071	0.0053	0.0057	**0.0181**
MAPE	UKF	0.0374	0.0547	0.0707	0.1628
	AUKF	0.0476	0.0466	0.0561	0.1503
	DI-ESN	0.0169	0.0074	0.0056	0.0299
	BI-LSTM	0.0190	0.0088	0.0054	0.0332
	Proposed method	0.0065	0.0053	0.0060	**0.0178**
$\%Er_{RUL}$	UKF	-	-	-	-
	DI-ESN	-	-	-	-
	BI-LSTM				-
	AUKF	-0.7718	1.4529	-0.8389	3.0636
	Proposed method	-0.5436	0	0	**-0.5436**

Because of inaccuracy estimation of SOH in the historical stage, it is difficult for AUKF to give accurate prediction for RUL. The proposed method provides accurate RUL prediction for FC3. Compared to AUKF, when TP is 60%, the precision is improved by 29.57%. When TP is 70% or 80%, the RUL prediction deviates little from the real value.

The proposed method can predict the degradation trend well with different TPs. In terms of stacked RMSE, compared with UKF, AUKF, DI-ESN and Bi-LSTM, the errors of the proposed method are reduced by 88.12%, 41.99%, 13.82% and 3.21%, respectively. It indicates that the proposed method can make good degradation prediction under the dynamic condition.

D. RUL prediction

The Satisfactory Horizon (SH) is defined as the duration in which the predicted RUL values fall within an acceptable error range [26]. The results of RUL prediction for the entire lifecycle are shown in Fig.11.

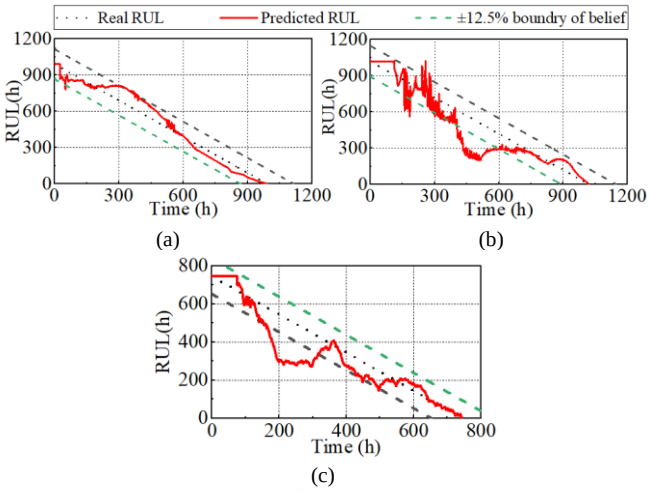

Fig.11 RUL predictions of the proposed method. (a) FC1. (b) FC2. (c) FC3.

TABLE V.
COMPARISON OF RUL PREDICTION

PEMFC	Metrics	PF [49]	UKF	AUKF	Proposed method
FC1	*Acc*	0.8100	0.7379	0.6599	**0.8341**
	SH(h)	-	970	570	919
FC2	*Acc*	0.6330	0.5938	0.546	**0.7344**
	SH(h)	-	504	461	771
FC3	*Acc*	-	-	0.3766	**0.7919**
	SH(h)	-	-	313	577

The RUL prediction curve for FC1 is relatively smooth. However, for FC2, the presence of faults causes a significant reduction in experimental data. This results in noticeable fluctuations in the predicted RUL. The SH for FC2 is decreased by 14.92% and the accuracy is decreased by 11.95% compared to FC1. The proposed method demonstrates a significant improvement in accuracy of RUL prediction compared to the other methods shown in TABLE V. For FC1, compared with PF [49], UKF and AUKF, the proposed method improves the accuracy by 2.98%, 13.03% and 26.40%, respectively. For FC2, the proposed method shows improvement of 16.02%, 23.67% and 34.51%. For FC3, the proposed method's RUL prediction has significant advantages over AUKF in terms of *Acc* and SH. The proportion of SH in the entire lifecycle has increased by 84.10%. RUL prediction accuracy of the proposed method is 110% higher than that of AUKF. This indicates that for the same model, the ability of the proposed method to quantify uncertainty behavior is superior to adaptive algorithm. Under the quasi-dynamic operating condition, it has improved by 2.28% compared to the best result in [49].

Robustness is as important as accuracy in RUL prediction for PEMFC. In Bayesian framework, initial state is the best estimation of the state of the system at the beginning of state estimation. This is a guess as to the state of the system at the initial moment [35]. The state covariance is a measure of uncertainty associated with the initial state estimation. It is necessary to obtain the initial state and the associated covariance based on prior information. The robustness can be validated by examining the performance of the method with different initial conditions including initial state and covariance of initial state [31].

Before the aging test begins, the fuel cell is considered to be brand new but it should have an aging trend, so SOH is set to 0, and the its rate of change may be variable. Initial state covariance should be variable due to variability of the prior information [31]. Therefore, the initial rate of change and values in the error covariance are adjusted. Five types are set: type 1 ($\boldsymbol{x}_0$=[0; 0.001], $\boldsymbol{P}_0$=[0.001, 0; 0, 0.001]), type 2 ($\boldsymbol{x}_0$=[0; 0.005], $\boldsymbol{P}_0$=[0.05, 0; 0, 0.05]), type 3 ($\boldsymbol{x}_0$=[0; 0.01], $\boldsymbol{P}_0$=[0.1, 0; 0, 0.1]), type 4($\boldsymbol{x}_0$=[0; 0.05], $\boldsymbol{P}_0$=[0.5, 0; 0, 0.5]) and type 5($\boldsymbol{x}_0$=[0; 0.1], $\boldsymbol{P}_0$=[1, 0; 0, 1]).

TABLE V.
RESULTS OF RUL PREDICTION BASED ON DIFFERENT INITIALIZATION

	FC1		FC2		FC3	
	Acc	SH	Acc	SH	Acc	SH
Type 1	0.8296	846	0.7298	753	0.7951	603
Type 2	0.7738	861	0.7235	725	0.7960	604
Type 3	0.7667	844	0.7197	697	0.7792	584
Type 4	0.8451	979	0.7205	809	0.7979	593
Type 5	0.8599	965	0.6702	692	0.7964	583

The proposed method can effectively forecast RUL. For FC1, *Acc* remains above 0.75, and for FC2, the *Acc* remains above 0.65. For FC3, *Acc* remains above 0.79. The average of FC1 is 0.815, which has a 14.35% increase in *Acc* compared to FC2. However, the proposed method exhibits the best prediction stability for FC3, with the smallest variance of 0.0006. And the variance of FC2 is smaller than that of FC1. The range of RUL prediction of FC3 is 21h, while FC1's is 135h and FC2's is 117h. The validation indicates that the proposed method achieves higher accuracy in scenarios with stronger linearity, like the static operating condition. And it can achieve better prediction stability in scenarios with higher uncertainty, like the dynamic operating condition.

V. Conclusion

Uncertainty in the PEMFC aging behavior model can significantly impacts the accuracy of RUL prediction and robustness. A Bayesian-based RUL prediction method for PEMFC that incorporates uncertainty quantification on the full-time scale is proposed. DBO-LSTM is used to quantify uncertainty behavior during the prediction stage. The method's advantages in RUL prediction accuracy and robustness are validated. The main conclusions are:

(1) For SOH estimation under the static, quasi-dynamic and dynamic operating conditions, the direction of state drift caused by uncertainty is [0, 1; 0, 0]. The degree of state drift under the dynamic condition is greatest. Under these operating conditions, the prediction for degree of state drift is accurate. The prediction errors are lower than 0.06, 0.0004, and 0.00015, respectively.

(2) The proposed method can achieve good long-term prediction. This advantage is particularly prominent in the dynamic condition. When TP is 60%, compared to AUKF, the relative error of RUL prediction is decreased by 29.57%. The *Acc* in the entire lifecycle is increased by 34.51%, respectively.

(3) Effective prediction for RUL can always be obtained, even with different initial conditions. Validation shows that the proposed method can achieve long-term prediction with higher precision under the static operating condition. Under the quasi-dynamic and dynamic operating conditions, the stability of the proposed method is better.

The proposed method can also be applied to the estimation and prediction of the state of charge and battery capacity in lithium batteries. In future work, we will investigate the application of the proposed method in PEMFC operation strategy research and fuel cell system control.

References

[1] K. He, C. Zhang, Q. He, Q. Wu, L. Jackson, and L. Mao, "Effectiveness of PEMFC historical state and operating mode in PEMFC prognosis," *International Journal of Hydrogen Energy*, vol. 45, no. 56, pp. 32355–32366, Nov. 2020, doi: 10.1016/j.ijhydene.2020.08.149.

[2] Z. Liu *et al.*, "Efficient fault diagnosis of proton exchange membrane fuel cell using external magnetic field measurement," *Energy Conversion and Management*, vol. 266, p. 115809, Aug. 2022, doi: 10.1016/j.enconman.2022.115809

[3] H. Wu, W. Wang, Y. Li, W. Zhu, C. Xie, and H. B. Gooi, "Hybrid physics-based and data-driven prognostic for PEM fuel cells considering voltage recovery," IEEE Trans. Energy Convers., pp. 1–11, 2023, doi: 10.1109/TEC.2023.3311460.

[4] J. Zhao and X. Li, "A review of polymer electrolyte membrane fuel cell durability for vehicular applications: Degradation modes and experimental techniques," *Energy Conversion and Management*, vol. 199, p. 112022, Nov. 2019, doi: 10.1016/j.enconman.2019.112022.

[5] S. Li, W. Luan, C. Wang, Y. Chen, and Z. Zhuang, "Degradation prediction of proton exchange membrane fuel cell based on Bi-LSTM-GRU and ESN fusion prognostic framework," *International Journal of Hydrogen Energy*, vol. 47, no. 78, pp. 33466–33478, Sep. 2022, doi: 10.1016/j.ijhydene.2022.07.230.

[6] A. Tang, Y. Yang, Q. Yu, Z. Zhang, and L. Yang, "A review of life prediction methods for PEMFCs in electric vehicles," *Sustainability*, vol. 14, no. 16, p. 9842, Aug. 2022, doi: 10.3390/su14169842.

[7] M. Bressel, M. Hilairet, D. Hissel, and B. Ould Bouamama, "Extended Kalman filter for prognostic of proton exchange membrane fuel cell," *Applied Energy*, vol. 164, pp. 220–227, Feb. 2016, doi: 10.1016/j.apenergy.2015.11.071.

[8] K. Chen, S. Laghrouche, and A. Djerdir, "Fuel cell health prognosis using Unscented Kalman Filter: Postal fuel cell electric vehicles case study," *International Journal of Hydrogen Energy*, vol. 44, no. 3, pp. 1930–1939, Jan. 2019, doi: 10.1016/j.ijhydene.2018.11.100.

[9] Y. Ao, S. Laghrouche, D. Depernet, and K. Chen, "Proton exchange membrane fuel cell prognosis based on frequency-domain Kalman filter," *IEEE Trans. Transp. Electrific.*, vol. 7, no. 4, pp. 2332–2343, Dec. 2021, doi: 10.1109/TTE.2021.3077506.

[10] L. He *et al.*, "A quick evaluation method for the lifetime of the fuel cell MEA with the particle filter algorithm," *International Journal of Green Energy*, vol. 18, no. 14, pp. 1536–1549, Nov. 2021, doi: 10.1080/15435075.2021.1911809.

[11] Y. Cheng, N. Zerhouni, and C. Lu, "A hybrid remaining useful life prognostic method for proton exchange membrane fuel cell," *International Journal of Hydrogen Energy*, vol. 43, no. 27, pp. 12314–12327, Jul. 2018, doi: 10.1016/j.ijhydene.2018.04.160.

[12] P. Wang *et al.*, "A novel degradation model of proton exchange membrane fuel cells for state of health estimation and prognostics," *International Journal of Hydrogen Energy*, vol. 46, no. 61, pp. 31353–31361, Sep. 2021, doi: 10.1016/j.ijhydene.2021.07.004.

[13] M. Jouin, R. Gouriveau, D. Hissel, M.-C. Péra, and N. Zerhouni, "Degradations analysis and aging modeling for health assessment and prognostics of PEMFC," *Reliability Engineering & System Safety*, vol. 148, pp. 78–95, Apr. 2016, doi: 10.1016/j.ress.2015.12.003.

[14] M. Messing and E. Kjeang, "Empirical modeling of cathode electrode durability in polymer electrolyte fuel cells," *Journal of Power Sources*, vol. 451, p. 227750, Mar. 2020, doi: 10.1016/j.jpowsour.2020.227750.

[15] A. Kneer and N. Wagner, "A semi-empirical catalyst degradation model based on voltage cycling under automotive operating conditions in PEM fuel cells," *J. Electrochem. Soc.*, vol. 166, no. 2, pp. F120–F127, 2019, doi: 10.1149/2.0641902jes.

[16] R. Ma, R. Xie, L. Xu, Y. Huangfu, and Y. Li, "A hybrid prognostic method for PEMFC with aging parameter prediction," *IEEE Trans.*

Transp. Electrific., vol. 7, no. 4, pp. 2318–2331, Dec. 2021, doi: 10.1109/TTE.2021.3075531.

[17] H. Zhen, W. Gong, and L. Wang, "Offline data-driven evolutionary optimization based on model selection," *Swarm and Evolutionary Computation*, vol. 71, p. 101080, Jun. 2022, doi: 10.1016/j.swevo.2022.101080.

[18] R. Mezzi, N. Yousfi-Steiner, M. C. Péra, D. Hissel, and L. Larger, "An Echo State Network for fuel cell lifetime prediction under a dynamic micro-cogeneration load profile," *Applied Energy*, vol. 283, p. 116297, Feb. 2021, doi: 10.1016/j.apenergy.2020.116297.

[19] R. E. Silva *et al.*, "Proton exchange membrane fuel cell degradation prediction based on Adaptive Neuro-Fuzzy Inference Systems," *International Journal of Hydrogen Energy*, vol. 39, no. 21, pp. 11128–11144, Jul. 2014, doi: 10.1016/j.ijhydene.2014.05.005.

[20] K. Chen, S. Laghrouche, and A. Djerdir, "Prognosis of fuel cell degradation under different applications using wavelet analysis and nonlinear autoregressive exogenous neural network," *Renewable Energy*, vol. 179, pp. 802–814, Dec. 2021, doi: 10.1016/j.renene.2021.07.097.

[21] Y. Wu, E. Breaz, F. Gao, and A. Miraoui, "A modified relevance vector machine for PEM fuel-cell stack aging prediction," *IEEE Trans. on Ind. Applicat.*, vol. 52, no. 3, pp. 2573–2581, May 2016, doi: 10.1109/TIA.2016.2524402.

[22] H. Deng *et al.*, "Degradation trajectories prognosis for PEM fuel cell systems based on Gaussian process regression," *Energy*, vol. 244, p. 122569, Apr. 2022, doi: 10.1016/j.energy.2021.122569.

[23] J. Liu, Q. Li, W. Chen, Y. Yan, Y. Qiu, and T. Cao, "Remaining useful life prediction of PEMFC based on long short-term memory recurrent neural networks," *International Journal of Hydrogen Energy*, vol. 44, no. 11, pp. 5470–5480, Feb. 2019, doi: 10.1016/j.ijhydene.2018.10.042.

[24] Y. Wang et al., "Degradation prediction of proton exchange membrane fuel cell stack using semi-empirical and data-driven methods," Energy and AI, vol. 11, p. 100205, Jan. 2023, doi: 10.1016/j.egyai.2022.100205.

[25] J. Jin, Y. Chen, C. Xie, W. Zhu, and F. Wu, "Remaining useful life prediction of PEMFC based on cycle reservoir with jump model," *International Journal of Hydrogen Energy*, vol. 46, no. 80, pp. 40001–40013, Nov. 2021, doi: 10.1016/j.ijhydene.2021.09.233.

[26] Z. Hua, Z. Zheng, E. Pahon, M.-C. Péra, and F. Gao, "A review on lifetime prediction of proton exchange membrane fuel cells system," *Journal of Power Sources*, vol. 529, p. 231256, May 2022, doi: 10.1016/j.jpowsour.2022.231256.

[27] K. He, L. Mao, J. Yu, W. Huang, Q. He, and L. Jackson, "Long-Term Performance Prediction of PEMFC Based on LASSO-ESN," *IEEE Trans. Instrum. Meas.*, vol. 70, pp. 1–11, 2021, doi: 10.1109/TIM.2021.3058365.

[28] C. Wang, Z. Li, R. Outbib, M. Dou, and D. Zhao, "A novel long short-term memory networks-based data-driven prognostic strategy for proton exchange membrane fuel cells," *International Journal of Hydrogen Energy*, vol. 47, no. 18, pp. 10395–10408, Feb. 2022, doi: 10.1016/j.ijhydene.2022.01.121.

[29] D. Zhou, A. Al-Durra, K. Zhang, A. Ravey, and F. Gao, "Online remaining useful lifetime prediction of proton exchange membrane fuel cells using a novel robust methodology," *Journal of Power Sources*, vol. 399, pp. 314–328, Sep. 2018, doi: 10.1016/j.jpowsour.2018.06.098.

[30] R. Pan, D. Yang, Y. Wang, and Z. Chen, "Performance degradation prediction of proton exchange membrane fuel cell using a hybrid prognostic approach," *International Journal of Hydrogen Energy*, vol. 45, no. 55, pp. 30994–31008, Nov. 2020, doi: 10.1016/j.ijhydene.2020.08.082.

[31] H. Liu, J. Chen, D. Hissel, and H. Su, "Remaining useful life estimation for proton exchange membrane fuel cells using a hybrid method," *Applied Energy*, vol. 237, pp. 910–919, Mar. 2019, doi: 10.1016/j.apenergy.2019.01.023.

[32] D. Zhou, F. Gao, E. Breaz, A. Ravey, and A. Miraoui, "Degradation prediction of PEM fuel cell using a moving window based hybrid prognostic approach," *Energy*, vol. 138, pp. 1175–1186, Nov. 2017, doi: 10.1016/j.energy.2017.07.096.

[33] L. Vichard, N. Y. Steiner, N. Zerhouni, and D. Hissel, "Hybrid fuel cell system degradation modeling methods: A comprehensive review," *Journal of Power Sources*, vol. 506, p. 230071, Sep. 2021, doi: 10.1016/j.jpowsour.2021.230071.

[34] H. Geng, M. A. Haile, and H. Fang, "SSUE: Simultaneous state and uncertainty estimation for dynamical systems," *Int J Robust Nonlinear Control*, vol. 31, no. 4, pp. 1068–1083, Mar. 2021, doi: 10.1002/rnc.5344.

[35] H. Fang, N. Tian, Y. Wang, M. Zhou, and M. A. Haile, "Nonlinear Bayesian estimation: from Kalman filtering to a broader horizon," *IEEE/CAA J. Autom. Sinica*, vol. 5, no. 2, pp. 401–417, Mar. 2018, doi: 10.1109/JAS.2017.7510808.

[36] W. Wan *et al.*, "Operating conditions combination analysis method of optimal water management state for PEM fuel cell," *Green Energy and Intelligent Transportation*, p. 100105, Jun. 2023, doi: 10.1016/j.geits.2023.100105.

[37] S. Zhou, P. R. Shearing, D. J. L. Brett, and R. Jervis, "Machine learning as an online diagnostic tool for proton exchange membrane fuel cells," *Current Opinion in Electrochemistry*, vol. 31, p. 100867, Feb. 2022, doi: 10.1016/j.coelec.2021.100867.

[38] Z. Ghahramani, "Probabilistic machine learning and artificial intelligence," Nature, vol. 521, no. 7553, pp. 452–459, May 2015, doi: 10.1038/nature14541.

[39] W. Zhu *et al.*, "Uncertainty quantification of proton-exchange-membrane fuel cells degradation prediction based on Bayesian-Gated Recurrent Unit," *eTransportation*, vol. 16, p. 100230, Apr. 2023, doi: 10.1016/j.etran.2023.100230

[40] H. Fang, T. Srivas, R. A. De Callafon, and M. A. Haile, "Ensemble-based simultaneous input and state estimation for nonlinear dynamic systems with application to wildfire data assimilation," *Control Engineering Practice*, vol. 63, pp. 104–115, Jun. 2017, doi: 10.1016/j.conengprac.2017.03.005.

[41] S. Z. Yong, M. Zhu, and E. Frazzoli, "A unified filter for simultaneous input and state estimation of linear discrete-time stochastic systems," *Automatica*, vol. 63, pp. 321–329, Jan. 2016, doi: 10.1016/j.automatica.2015.10.040.

[42] FCLAB Research. IEEE PHM 2014 data challenge. 2014. http://eng.fclab.fr/ieee- phm-2014-data-challenge/.

[43] R. Ma *et al.*, "Data-fusion prognostics of proton exchange membrane fuel cell degradation," *IEEE Trans. on Ind. Applicat.*, vol. 55, no. 4, pp. 4321–4331, Jul. 2019, doi: 10.1109/TIA.2019.2911846.

[44] J. Zuo *et al.*, "Long-term dynamic durability test datasets for single proton exchange membrane fuel cell," *Data in Brief*, vol. 35, p. 106775, Apr. 2021, doi: 10.1016/j.dib.2021.106775.

[45] C. Wang, M. Dou, Z. Li, R. Outbib, D. Zhao, and B. Liang, "A fusion prognostics strategy for fuel cells operating under dynamic conditions," *eTransportation*, vol. 12, p. 100166, May 2022, doi: 10.1016/j.etran.2022.100166.

[46] Zuo J, Lv H, Zhou D, Xue Q, Jin L, Zhou W, et al. Deep learning based prognostic framework towards proton exchange membrane fuel cell for automotive application. Applied Energy 2021;281:115937. https://doi.org/10.1016/j.apenergy.2020.115937.

[47] D. Spinello and D. J. Stilwell, "Nonlinear estimation with state-dependent gaussian observation noise," *IEEE Trans. Automat. Contr.*, vol. 55, no. 6, pp. 1358–1366, Jun. 2010, doi: 10.1109/TAC.2010.2042006.

[48] Z. Hua, Z. Zheng, M.-C. Péra, and F. Gao, "Remaining useful life prediction of PEMFC systems based on the multi-input echo state network," Applied Energy, vol. 265, p. 114791, May 2020, doi: 10.1016/j.apenergy.2020.114791.

[49] D. Zhang, C. Cadet, N. Yousfi-Steiner, and C. Bérenguer, "Proton exchange membrane fuel cell remaining useful life prognostics considering degradation recovery phenomena," *Proceedings of the Institution of Mechanical Engineers, Part O: Journal of Risk and Reliability*, vol. 232, no. 4, pp. 415–424, Aug. 2018, doi: 10.1177/1748006X18776825.